X-913-75-252
PREPRINT

NASA TM X- 71000

SATELLITE MICROWAVE OBSERVATIONS OF THE UTAH GREAT SALT LAKE DESERT

OCTOBER 1975

GSFC

GODDARD SPACE FLIGHT CENTER
GREENBELT, MARYLAND

SATELLITE MICROWAVE OBSERVATIONS OF THE

UTAH GREAT SALT LAKE DESERT

Fawwaz T. Ulaby and Louis F. Dellwig
University of Kansas Center for Research, Inc.
Remote Sensing Laboratory
Lawrence, Kansas 66045

Thomas Schmugge
NASA Goddard Space Flight Center
Hydrology and Oceanography Branch
Greenbelt, Maryland 20771

ABSTRACT

Microwave data acquired over the Great Salt Lake Desert area by sensors aboard Skylab and Nimbus 5 indicate that the microwave emission and backscatter were strongly influenced by contributions from subsurface layers of sediment saturated with brine. This phenomenon was observed by Skylab's S-194 radiometer operating at 1.4 GHz, S-193 RADSCAT (Radiometer-Scatterometer) operating at 13.9 GHz and the Nimbus 5 ESMR (Electrically Scanning Microwave Radiometer) operating at 19.35 GHz. The availability of ESMR data over an 18 month period allowed an investigation of temporal variations. Aircraft 1.4 GHz radiometer data acquired two days after one of the Skylab passes confirm the satellites' observations. ESMR data reveal similar responses over the Bolivian deserts, which have geologic features similar to those of the Utah desert.

TABLE OF CONTENTS

LIST OF FIGURES

LIST OF FIGURES (continued

1.0 INTRODUCTION

The microwave emissivity, ϵ, and backscattering coefficient, σ^o, of terrain surfaces are functions of the dielectric properties and surface roughness (relative to the wavelength) of the ground. The dielectric properties are in turn strongly influenced by the soil moisture content. Microwave observations of soil surfaces by active [Ulaby, 1974a,b; Ulaby et al., 1975a] and passive [Schmugge et al., 1974; Newton et al., 1974; Eagleman and Ulaby, 1974] sensors indicate a high degree of sensitivity to soil moisture variations. Due to the nature of the scattering and emission phenomena, the scattering coefficient exhibits a positive correlation with soil moisture content, whereas the emissivity (and hence brightness temperature) decreases with soil moisture content. In both cases [Ulaby et al., 1975a; Newton et al., 1974] longer wavelengths have been observed to yield more satisfactory results (in terms of sensitivity to moisture variations) simply because, for a given terrain surface, the effects of surface roughness on the microwave response (backscatter and emission) are reduced as the wavelength is made longer since the surface would appear electromagnetically smoother.

Brightness temperature data acquired by Skylab and Nimbus 5 microwave radiometers over Utah indicate a consistent difference in temperature between the Great Salt Lake Desert area and neighboring land surfaces. The Skylab microwave sensors include a 13.9 GHz Radiometer-Scatterometer (RADSCAT) designated S-193 and a L-band radiometer operating at 1.4 GHz designated S-194. The microwave sensor aboard Nimbus 5 is a 19.35 GHz Electrically Scanning Microwave Radiometer (ESMR).

During Skylab Pass 5 on June 5, 1973, S-193 measured brightness temperature values as low as 200°K for some parts of the Great Salt Lake Desert in comparison to a 270°-280°K range for areas outside the desert. In conjunction with the low temperature values, the measured scattering coefficient of the same general area was more than 15 dB higher than the scattering coefficient of areas outside the desert. Similar observations to those indicated by the S-193 radiometer were also evident in the data acquired by S-194 and ESMR for the same date. Another Skylab pass on August 8, 1973 and numerous ESMR passes over an 18 month period confirm that these observations are in response to specific characteristics of the Great Salt Lake Desert soil material. Detailed analysis of the data and the hydrology of the region has led us to believe that a significant contribution to the measured emitted and backscattered energy is from subsurface layers of brine.

As will be discussed in this paper, the availability of microwave data over the Great Salt Lake Desert at three different wavelengths has proven very useful in the analysis and interpretation. Moreover, the scatterometer data at 13.9 GHz has also served to complement the observations made with the passive sensors. The daily global coverage of the Nimbus 5 ESMR make possible observation of other salt deserts. In particular, low brightness temperatures have been observed over the salt deserts of the Alti Plano region of Bolivia.

2.0 DEVELOPMENT AND CHARACTERISTICS OF THE GREAT SALT LAKE DESERT

The test site under investigation trends in a northwest-southeast direction across the Great Salt Lake Desert (Figure 1). The narrow side represents the coverage on the ground by S-193 RADSCAT as the antenna was scanned in the cross-track-contiguous mode at 0° forward pitch during the Skylab June 5, 1973 descending pass (northwest to southeast direction) over Utah. S-194 coverage comprised approximately 74 per cent of the test site and complete coverage by ESMR is available for numerous passes. Two lines are shown in Figure 1, a horizontal line representing a transect across the desert at 40° 30' North latitude, the elevation profile of which is shown in Figure 2, and a NW-SE line indicating the coverage by the NASA airborne 1.4 GHz radiometer flown on August 10, 1973. Several types of terrain are also shown including lakes (Great Salt Lake and Utah Lake), saltflats, mud flats, mountains, and the Great Salt Lake Desert.

2.1 Hydrologic Properties

Fifteen to twenty thousand years ago, coincident with the beginning of the retreat of the most recent glacial advance over the northern portion of the North American continent, a large area of northwestern Utah was covered by ancient Lake Bonneville which, through a complex history of contractions and expansions, ultimately was reduced to the 4270 km^2 now occupied by the Great Salt Lake. To the southwest of the lake and connected to it by a narrow threshold is the Great Salt Lake Desert (Figure 1), approximately 9 m above the present level of the lake. Until approximately 10,000 years ago [Eardley, 1962], this area was covered by the waters of Lake Bonneville into which were washed the sediments now composing the lake bed deposits which underlie the salt encrusted surface. These deposits underlie the major portion of the Great Salt Lake Desert below altitudes of approximately 1300 meters

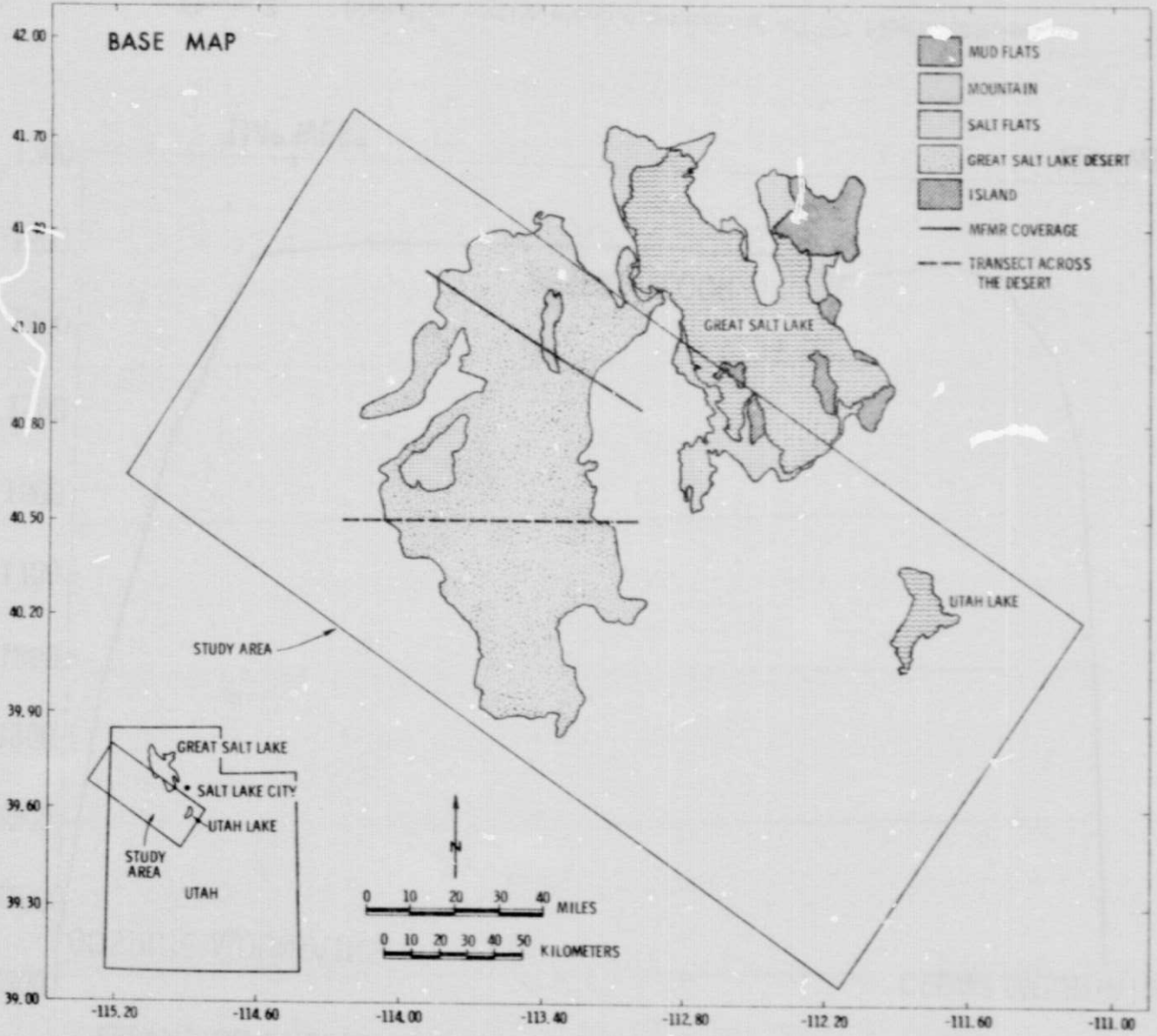

Figure 1. Great Salt Lake Desert test site. Elevation profile of the horizontal transect is shown in Figure 2 and the MFMR coverage refers to Figure 9.

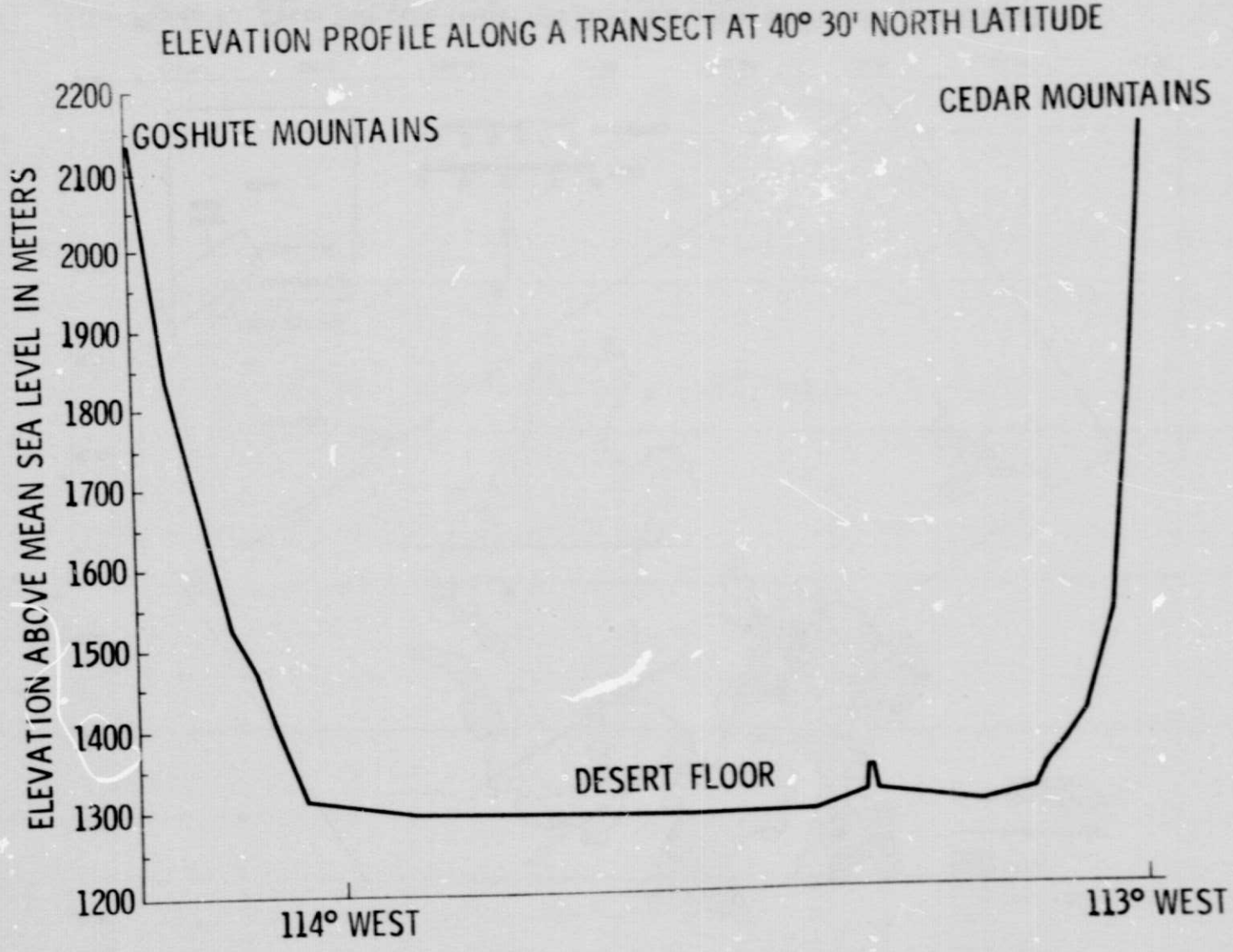

Figure 2. Elevation profile along a transect at 40°30' North latitude.

and are predominately clay and silt with variable salt content [Stephens, 1974]. From this bleak terrain surface rimmed by mountains (Figure 2) several areas show deviation: to the west in the general vicinity of Wendover, Utah lay the Bonneville Salt Flats and along the east side of the desert are gypsum sand dunes which have developed through the ablation of the desert surface by the westerly winds. In addition, isolated masses of bedrock protrude upward from the central and marginal areas of the Great Salt Lake Desert.

Lake bed clays and silts and crystalline salt form a shallow brine aquifer a maximum of 7.6 meters thick which covers the bulk of the surface of the Great Salt Lake Desert (Figure 3), only the northern portion of which has been studied in detail [Stephens, 1974].

Generally, in the area where lake clays form the surface, the depth to brine is estimated to range between 60 and 90 cm near the center of the desert floor and 2.1 - 2.7 m at the margins [Nolan, 1928], although capillary action in the fine grained sediments may raise the water in excess of one-half meter above the water table which causes the surface to remain perpetually moist. In the Bonneville Salt Flats, although the surface of the salt bed is rigid, the salt remains saturated with brine to within a few inches of the surface [Stephens, 1974], the water table ranging between approximately 15 and 20 cm below the surface. With the precipitation in the central part of the desert averaging less than 13 cm per year, the possibility of accumulating standing water on the desert surface or of elevating the water table above its normal 60-90 cm position below the desert's surface is minimal. Runoff from the highest parts of the mountains in the area averages less than 2.5 cm annually [Bridgley et al., 1964; Busby, 1966] and runoff during the brief periods of rapid snow melt generally infiltrates the stream channels downslope and only locally spreads out over the desert floor, most frequently in the Bonneville Salt Flats area. Recharge is by infiltration of precipitation and lateral subsurface inflow, the brine moving through the lake beds by intergrannular flow through layers of salt impregnated clay and through open joints (Figure 4).

2.2 Dielectric Properties

Except for a few isolated segments, the Great Salt Lake Desert is characterized by a very flat surface. Hence, as a first order approximation, the specular surface model can be applied to calculate the emissivity of the surface in terms of the power reflection coefficient R [Moore, 1975];

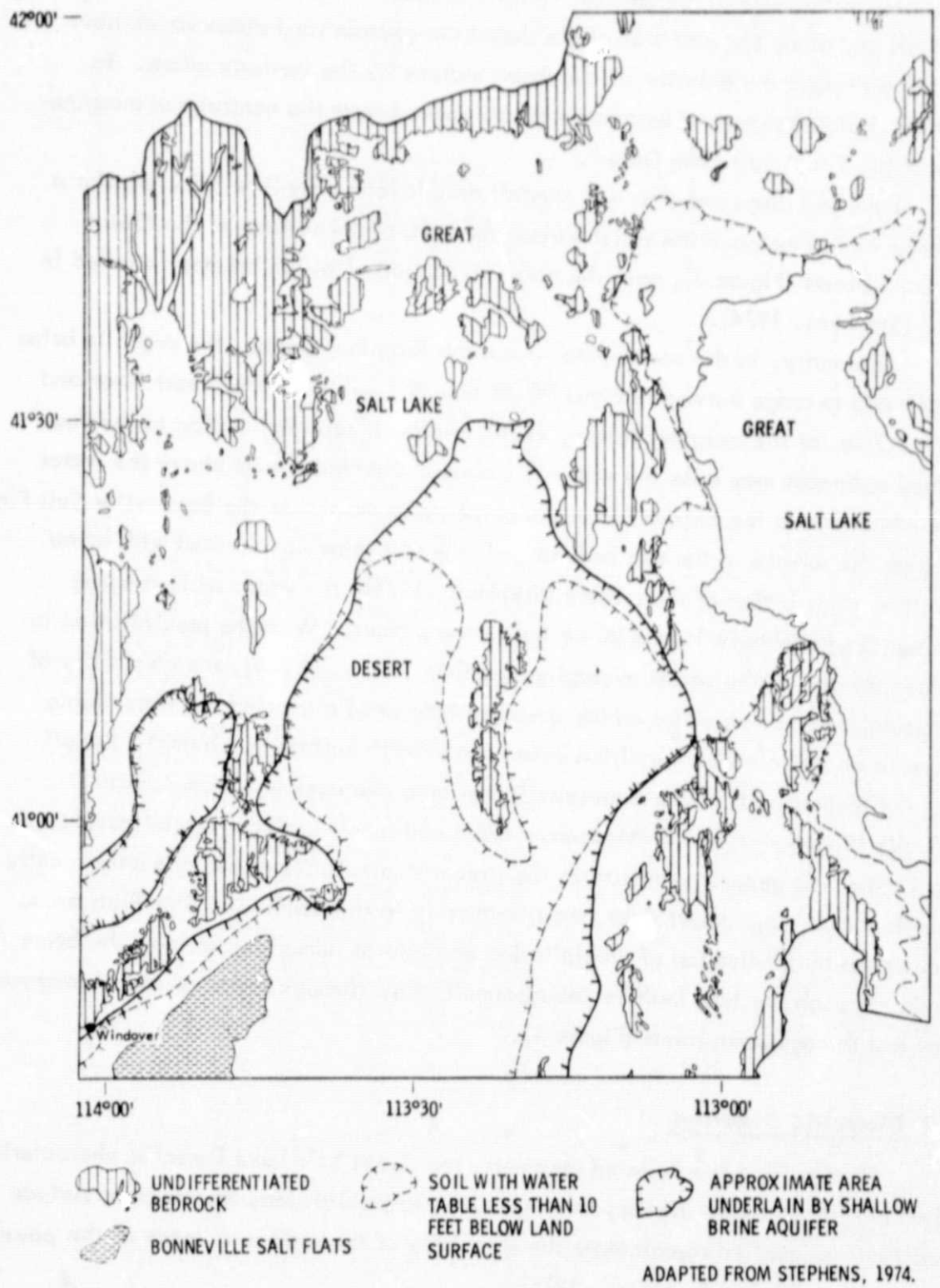

Figure 3. Northern portion of the Great Salt Lake Desert.

INFERRED SUBSURFACE STRATIGRAPHIC RELATIONSHIPS NEAR WENDOVER

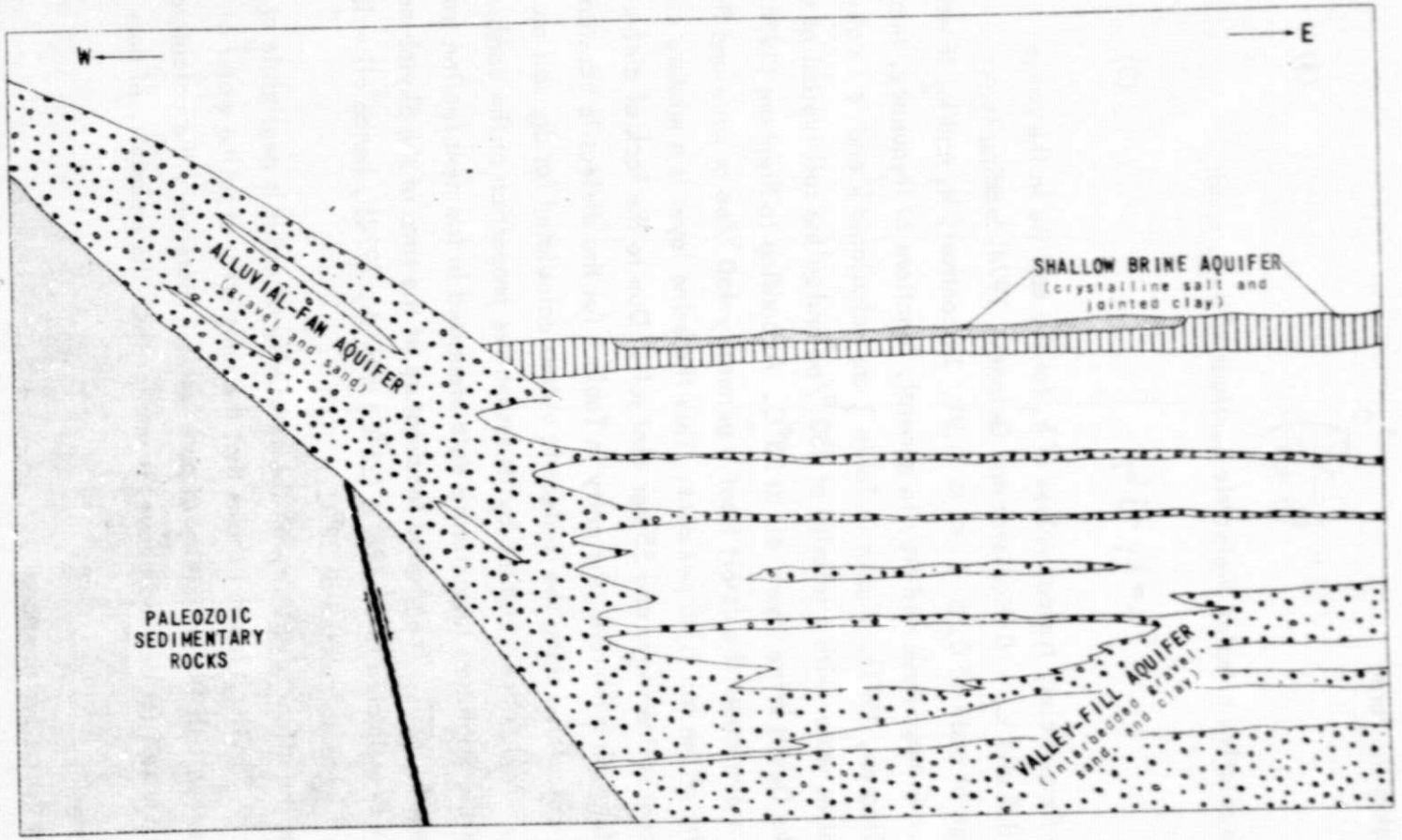

From Stephens, 1974.

Figure 4. Inferred subsurface stratigraphic relationships near Wendover, Utah.

$$\epsilon = 1 - R \qquad (1)$$

At nadir, R takes the form:

$$R = \left(\frac{1-\sqrt{k}}{1+\sqrt{k}}\right)^2 \qquad (3)$$

where k is the relative complex dielectric constant of the ground:

$$k = k_1 - j\,k_2 \qquad (3)$$

At microwave frequencies, typical values of k_1 for dry soil lie in the range $2.5 \leq k_1 \leq 3.5$ and $k_2 \approx 0$ [Hoekstra and Delaney, 1974] leading to an emissivity range at nadir of $0.95 \leq \epsilon \leq 0.91$. In contrast, k_1 and k_2 of water are much larger in magnitude and are, in general, functions of frequency, temperature and salinity [Stogryn, 1971]. Shown in Table 1 are calculated k and ϵ values for pure water, saline water with a salinity of 150 °/oo* and saline soil typical of the Great Salt Lake Desert brine layer, all at 23°C. According to Stephens [1974] the salinity of the water under the desert floor is generally 150 °/oo or more and the average porosity of the soil is 45 per cent. Thus the brine layer is a mixture consisting of 45 per cent saline water and 55 per cent soil. Due to the lack of dielectric constant data for such a mixture, the entry in Table 1 for the dielectric constant of saline soil was calculated using the dielectric values calculated for dry soil and saline water [Stogryn, 1971], each weighted by its respective proportion of the combined mixture.

Most of the brightness temperature data presented in the next section was acquired on June 5, 1973. The ground temperature at the time of the Skylab and Nimbus passes was estimated to be 296°K (23°C) [NASA, 1974], hence all values shown in Table 1 were calculated at 23°C.

Whereas the effect of salinity on the emissivity of water is negligible at 13.9 GHz and 19.35 GHz, Table 1 shows that the emissivity of saline water at 1.4 GHz is less than half the emissivity of pure water. Moreover, the calculated emissivity of saline soil (as defined above) is smaller than the emissivity of pure water

---

* °/oo stands for "parts per thousand".

Table 1. Calculated dielectric constant k and emissivity ϵ of dry soil, pure water, saline water and saline soil at 23°C.

	Dry Soil		Pure Water		Saline Water*		Saline Soil**	
Frequency	k_d	ϵ_d	k_p	ϵ_p	k_s	ϵ_s	k_{ss}	ϵ_{ss}
1.4 GHz	3-j0	0.928	78.63-j5.57	0.364	41.9-j237.4	0.179	20.5-j106.8	0.256
13.9 GHz	3-j0	0.928	52.4-j35.7	0.382	31.4-j40.6	0.394	15.7-j18.3	0.524
19.35 GHz	3-j0	0.928	40.4-j37.2	0.396	25.7-j35.6	0.416	13.2-j16.0	0.549

*Salinity = 150 °/oo

**$k_{ss} = 0.55\, k_d + 0.45\, k_s$

3.0 MICROWAVE OBSERVATIONS

At satellite altitudes, the measured brightness temperature of a flat surface is given by [Moore, 1975]:

$$T_B = \tau_a [T_{BS} + (1 - \epsilon) T_d] + T_u \qquad (4)$$

where τ_a is atmospheric transmittance, T_{BS} is the brightness temperature of the surface, T_d is the brightness temperature of the total downward radiation (atmospheric plus cosmic) and T_u is the brightness temperature of the upward atmospheric radiation. T_{BS} is the product of ϵ and the ground thermometric temperature T_g. Under clear sky conditions, atmospheric effects are negligible for the dry desert atmosphere of the Great Salt Lake Desert area, particularly at 1.4 GHz and 13.9 GHz. After calculating τ, T_u and T_d for the June 5, 1973 atmospheric conditions, the error between the measured brightness temperature T_B and the brightness temperature of the surface T_{BS}:

$$\Delta T = T_B - T_{BS} = T_B - \epsilon T_g \qquad (5)$$

was estimated by calculating ϵ using Eq. 4 for the range of values of T_B measured by the satellite radiometers. The following results were obtained:

$$\Delta T = \left\{ \begin{array}{ll} \leq 2.3^\circ K & \text{at 1.4 GHz} \\ \leq 2.5^\circ K & \text{at 13.9 GHz} \\ \leq 4.1^\circ K & \text{at 19.35 GHz} \end{array} \right\}$$

Similar results (within 0.2°K) were also obtained for the August 8, 1973 Skylab and Nimbus 5 passes over the Great Salt Lake Desert. In addition to these two passes, data reported herein includes Nimbus coverage over a period of 18 months during which the data acquired on some passes were more severely influenced by atmospheric conditions. During the drier winter months, calculations for the mid-latitude winter standard atmosphere profiles yield a smaller difference, $\Delta T \leq 5.9^\circ K$. The value of the difference for the Bolivian salt desert would be less than 5°K due to the higher altitude and reduced water vapor content.

If we model the Great Salt Lake Desert as a stratified medium consisting of a relatively dry surface layer of height h (layer 1) covering a substrate consisting of

saline soil (layer 2) with both layers having the same thermometric temperature T_g, the brightness temperature of the surface can be expressed as (adapted from King [1970]):

$$T_{BS} = T_g \, (1 - R_{1a}) \, (1 - \tau_1^2 \, R_{12}) \qquad (6)$$

where R is the power reflection coefficient at the interface between two semi-infinite homogeneous media. The subscript "a" refers to the air medium above layer 1. The effect of the attenuation by layer 1 is accounted for by the transmittance τ_1:

$$\tau_1(h) = \exp \, (- 2\alpha h) \qquad (7)$$

where 2α is the power attenuation coefficient of layer 1.

In the absence of the top layer, $R_{1a} = 0$, $R_{12} = R_{a2}$ and $\tau_1 = 1$ which leads to:

$$T_{BS} = T_g \, (1 - R_{a2})$$

$$= T_g \quad \epsilon_{a2}$$

where in this case ϵ_{a2} is the same as the emissivity of saline soil ϵ_{ss} (Table 1). Since α varies directly with frequency, the effect of attenuation by the top layer would be expected to be negligible at 1.4 GHz in comparison to 13.9 GHz and, especially, 19.35 GHz. Moreover, since h, the depth to brine, varies between about 10 cm near the center of the desert floor and 2.7 m at the margins, the effect of this variation should be reflected in the difference between the measured brightness temperature T_B and the brightness temperature of saline soil, $T_g \, \epsilon_{ss}$. Due to the lack of exact information on the moisture, salinity and temperature profiles of the Great Salt Lake Desert floor, only qualitative comparisons can be made between the measured brightness temperatures and the inferences drawn from the two-layer model discussed above.

Table 2 is a summary of vehicle, sensor, and test site parameters pertinent to the present study. More detailed information is given in each of the following subsections.

3.1 S-193 Observations

Three different microwave sensors operating at the same frequency of 13.9 GHz are incorporated in S-193: a radiometer, a scatterometer and an altimeter, all sharing the same antenna and some of the receiver front-end. In general, for a given pass (or

Table 2. Summary of Vehicle, Sensor, Pass and Site Information.

	S-194		S-193 RAD		S-193 SCAT		ESMR
Vehicle	Skylab		Skylab		Skylab		Nimbus 5
Altitude	438 km		438 km		438 km		1100 km
Sensor	Radiometer		Radiometer		Scatterometer		Radiometer
Frequency	1.4 GHz		13.9 GHz		13.9 GHz		19.35 GHz
Effective Antenna Beamwidth	15.2°		2.02°		1.56°		*
Beam Scanning	None		Mechanical		Mechanical		Electrical
Pass Information							
Pass Number	5	16	5	16	5	16	*
Pass Date	6-5-73	8-8-73	6-5-73	8-8-73	6-5-73	8-8-73	*
Local Time	10:58 a.m.	9:01 a.m.	10:58 a.m.	9:01 a.m.	10:58 a.m.	9:01 a.m.	12:00-1:00 p.m
Mode	nadir looking	nadir looking	CTC	CTC	CTC	CTC	CTC
Pitch Angle	0°	0°	0°	17.0°	0°	17.0°	0°
Scan Angle	N/A	N/A	± 10.5°	+10.5°	± 10.5°	± 10.5°	± 50°
Nadir Angle Range	N/A	N/A	0°- 10.5°	17.0°-20.0°	0°- 10.5°	17.0°-20.0°	0°-50°
Ground Resolution at 0° Scan Angle	117 km diameter	117 km diameter	15.5 km diameter	16.2 km x 16.9 km	11.11 km diameter	11.6 km x 12.1 km	25 km diameter
Ground Resolution at End of Scan	N/A	N/A	15.7 km x 16.0 km	16.5 km x 17.5 km	11.3 km x 11.4 km	11.8 km x 12.5 km	160 km x 45 km
Test Site Ground Temperature	296°K	298°K	296°K	298°K	296°K	298°K	*
General Reference	NASA (1974)		Sobti (1973)		Sobti (1973)		Wilheit (1972)

*see section 3.3

**CTC = Cross-Track-Contiguous

parts thereof) either the altimeter or the RADSCAT (Radiometer-Scatterometer) was operated. For the RADSCAT portion several modes of operation were available; each mode specifies the data taking sequences in terms of pitch and roll angles, polarization and sensor. Because of either coverage, incident angle and/or scanning mode considerations, only two S-193 passes were judged suitable for the purposes of the present study. These are Pass 5 on June 5, 1973 and Pass 16 on August 8, 1973. Detailed discussion of the data recorded on Pass 5 will be presented next followed by a brief summary of the observations noted from the data of Pass 16.

Pass 5 was a North-West to South-East descending pass during which S-193 RADSCAT was operated in a cross-track contiguous mode with the radiometer and scatterometer measurements interlaced in time. Other mode parameters include: linear polarization in a direction parallel to the spacecraft velocity vector, approximately 0° pitch, and roll scan between $+10.5^{\circ}$ and -10.5° relative to nadir in the cross-track direction. In this mode, the signal polarization relative to the ground is horizontal. During each scan 12 data points are recorded by each sensor. Figure 5 shows the radiometer footprints (calculated on the basis of the antenna beamwidth) enclosed in the test site frame chosen for this investigation. For reference considerations, the scans have been designated by alphabetical letters and the footprints within each scan are numbered. The position accuracy of the center of a footprint is estimated to be approximately equal to one half of a footprint diameter.

In Figure 5, scans a-d, which fall completely outside the desert area, show brightness temperatures between 270°K and 279°K. As the spacecraft moved towards the south-east, lower T_B values were observed over the desert, the lowest being 200°K at footprints 6h and 8h, situated approximately in the central part of the desert. Furthermore, the radiometer shows a drastic change as it crosses boundaries; viz., 3g (264°K) outside the desert, 4g (220°K) at the boundary, and 5g (206°K) inside the desert. In scan m, as the antenna scanned between 10m and 12m, two different boundaries are crossed; 10m is at 260°K, 11m is 205°K (saltflats) and 12m is 154°K (lake). Keeping in mind the position accuracy of these footprints and the topographic accuracy of the terrain map, it is clear that the radiometer response is fairly consistent throughout. Consider, for example, footprint 10S. Its relatively low brightness temperature of 198°K leads us to suspect that a larger portion of Utah Lake is enclosed in 10S than is shown.

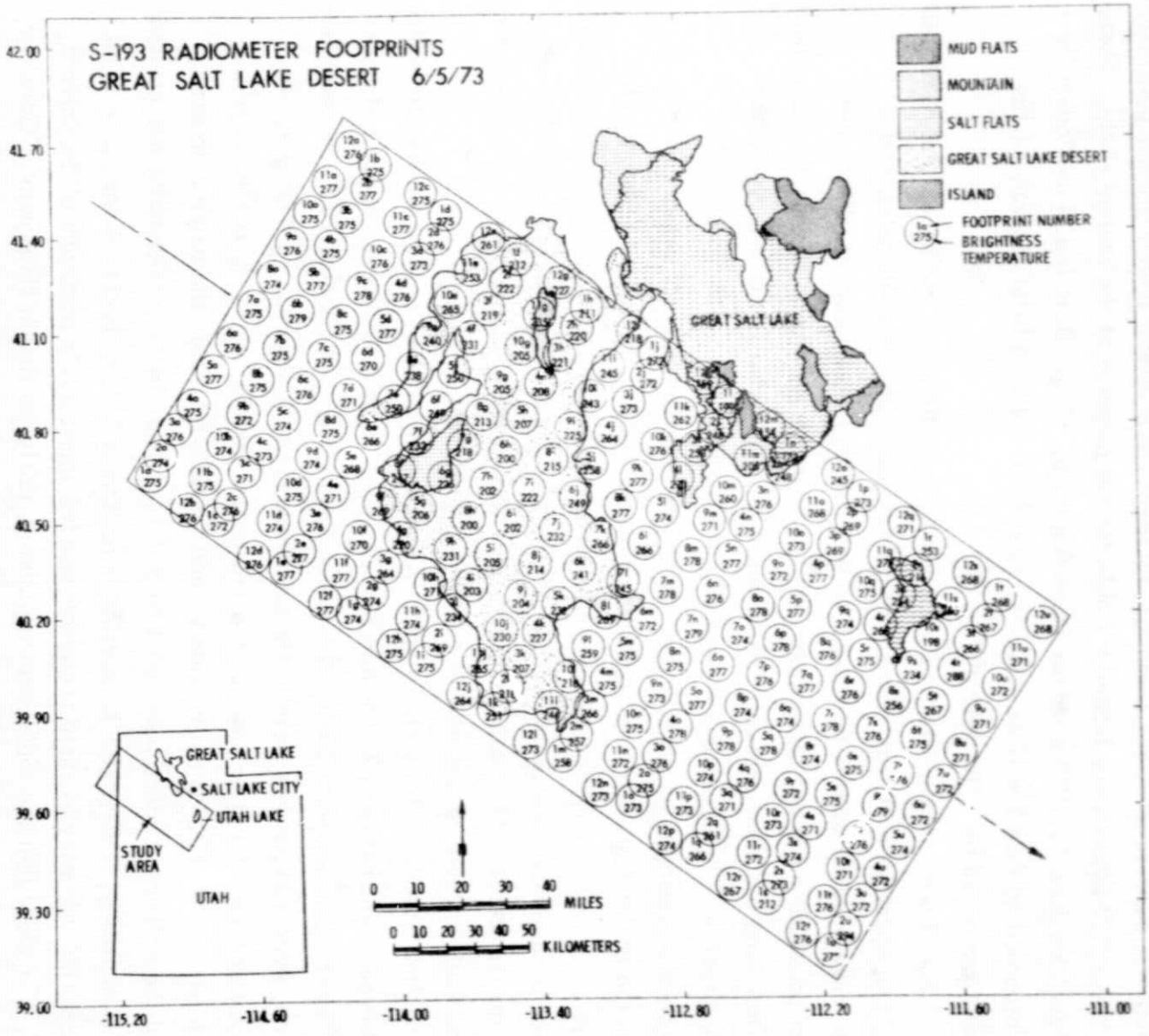

Figure 5. S-193 radiometer footprints, Pass 5, 6/5/73.

For a closer understanding of the spatial variation of the brightness temperature within the Great Salt Lake Desert area, Figure 6 shows a contour map generated on the basis of the data shown in Figure 5. Based on our earlier discussion of the desert hydrology, we propose that the contour map represents a gross "mapping" of the depth to the brine layer beneath the surface.

Whereas the microwave emissivity is almost insensitive to incident angle variation between nadir and 10.5°, the radar scattering coefficient experiences its largest drop in magnitude in precisely this range of angles. Hence for the purposes of this study, only the data within the $\pm$ 2.5° range around nadir was included in the contour map of Figure 7. The radar data confirms the observations made by the radiometer in that its measured scattering coefficient changes from values smaller than 0 dB for footprints outside the desert to values as high as 17.7 dB over the central part of the desert.

During the early stages of this study, it was suggested that perhaps the response observed by S-193 over the Great Salt Lake Desert might be due to spots of standing water formed by a previous rainfall. No such evidence was observed on the Skylab photography (S 190A) of this area. The next step was to determine whether or not this phenomenon is also evident from data acquired by a) other Skylab passes or b) other satellites carrying microwave sensors. The answer to the latter was provided by ESMR (section 3.3) while the answer to the earlier was provided by Skylab Pass 16 on August 8, 1973, approximately two months after Pass 5. The subsatellite track of Pass 16 was approximately parallel to that of Pass 5 but was shifted towards the North-East by about 52 km.

During Pass 16 over Utah, S-193 RADSCAT was operated in a cross-track contiguous mode similar to Pass 5, except that the pitch angle was about 17° (0° for Pass 5). Corresponding to a roll scan of $\pm$ 10°, the incident angle varied between about 17° (at 0° roll) and 20° (at 10° roll). Thus, for all practical purposes, the incident angle was almost a constant. Due to the larger pitch angle employed in Pass 16, the scatterometer and radiometer footprints were slightly larger (than those of Pass 5). The Pass 16 data were used to generate footprint and contour maps similar to those shown in Figures 5 and 6. Over the test site area, the radiometer recorded a high of 273°K and a low of 199°K [Figures 8 and 9]. The general shape of the contours are similar to those produced from the June 5, 1973 data. Footprints over the Salt Lake itself recorded brightness temperatures as low as 146°K. The point to be made here is that indeed the phenomenon observed in June was also evident in August.

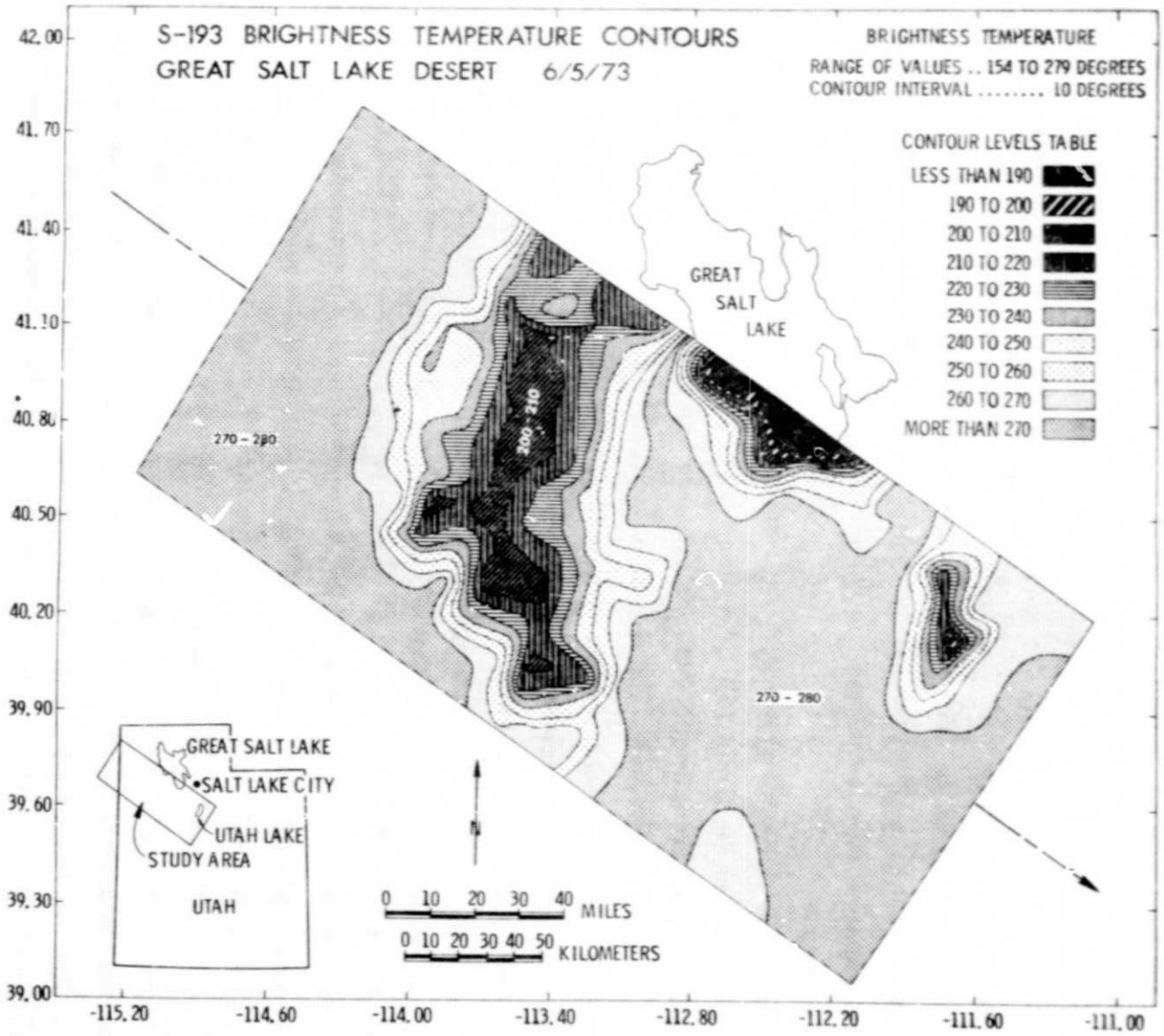

Figure 6. S-193 brightness temperature contours based on the data of Figure 5.

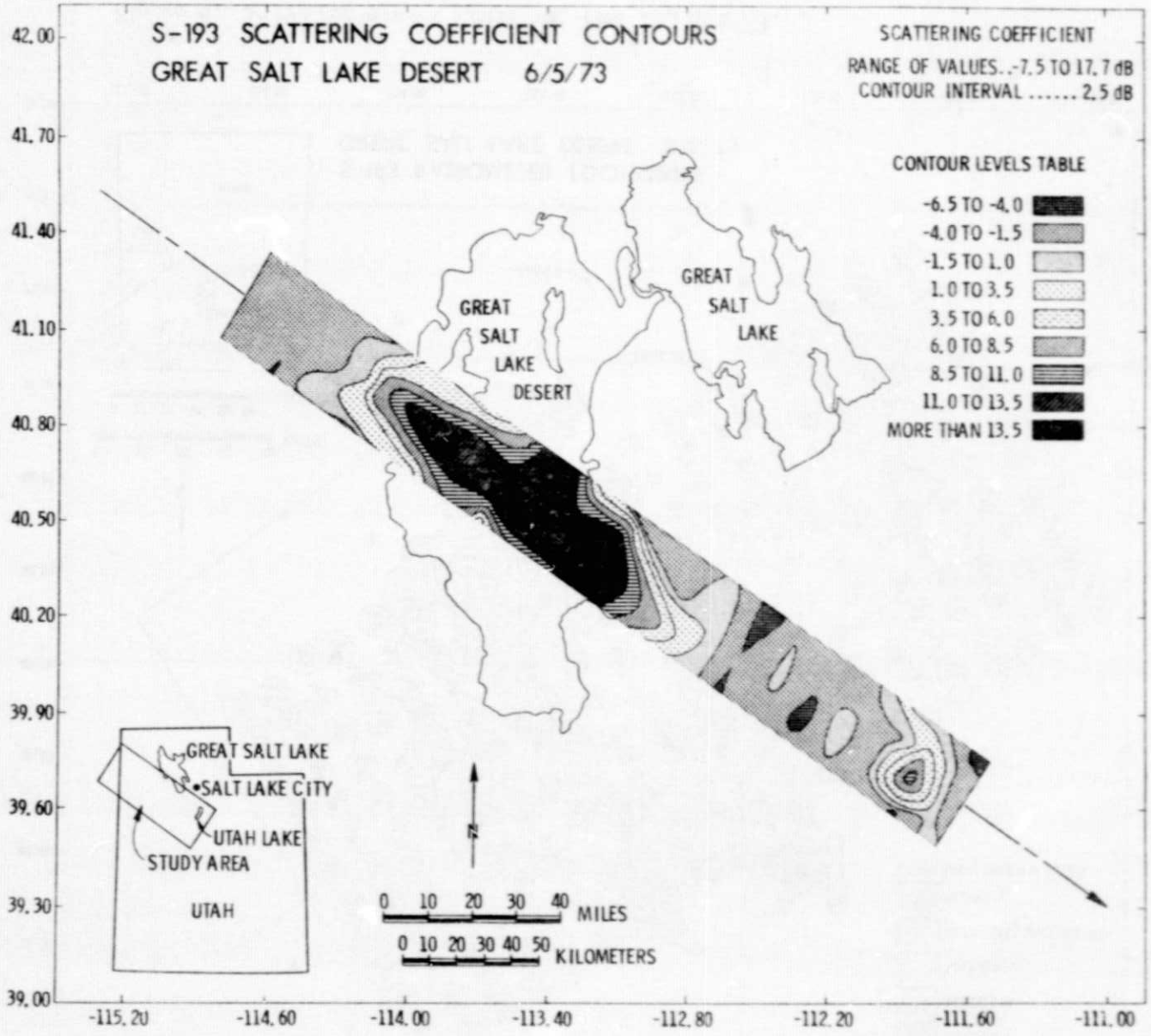

Figure 7. S-193 scattering coefficient contours, Pass 5, 6/5/73.

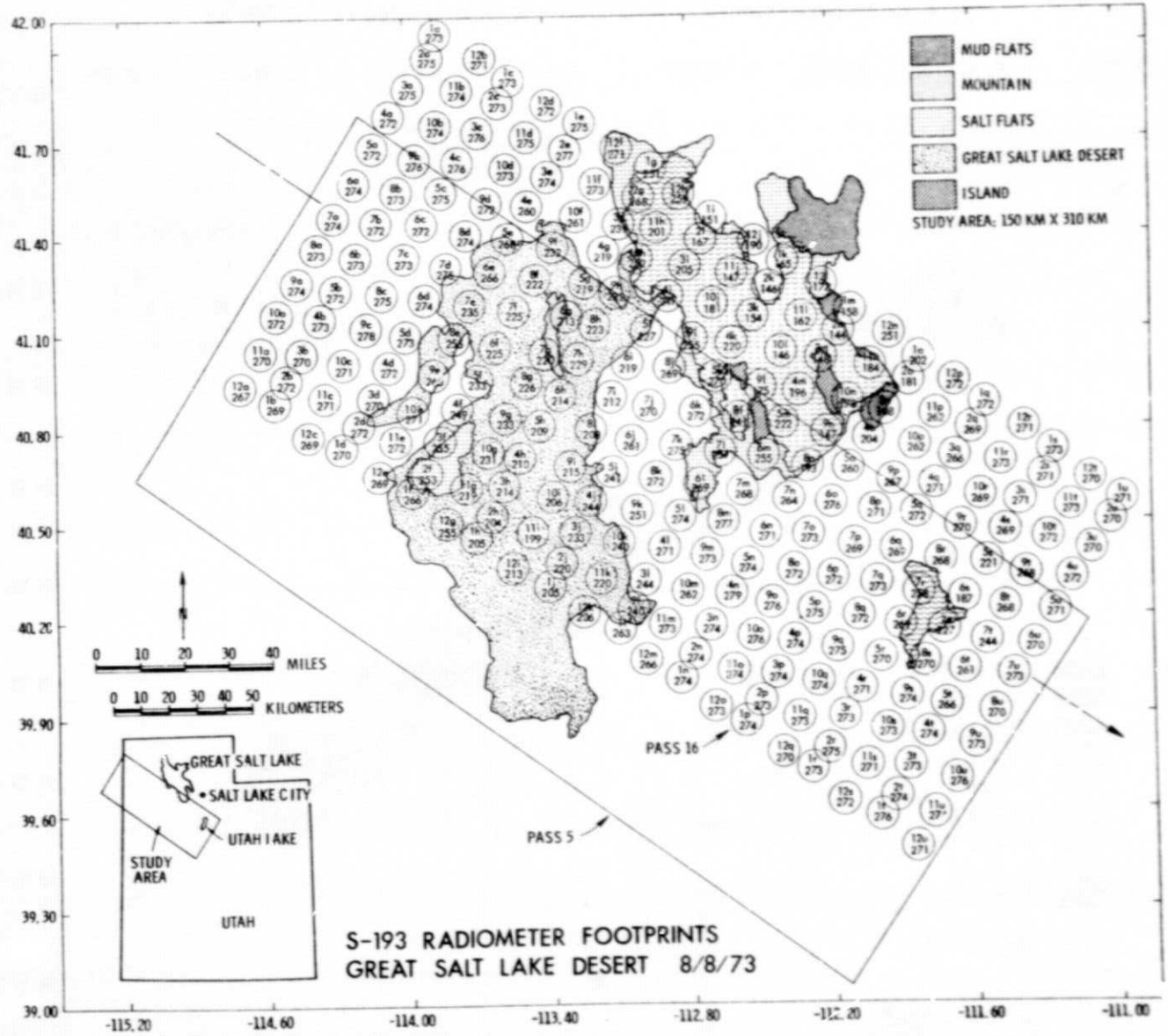

Figure 8. S-193 radiometer footprints, Pass 16, 8/8/73.

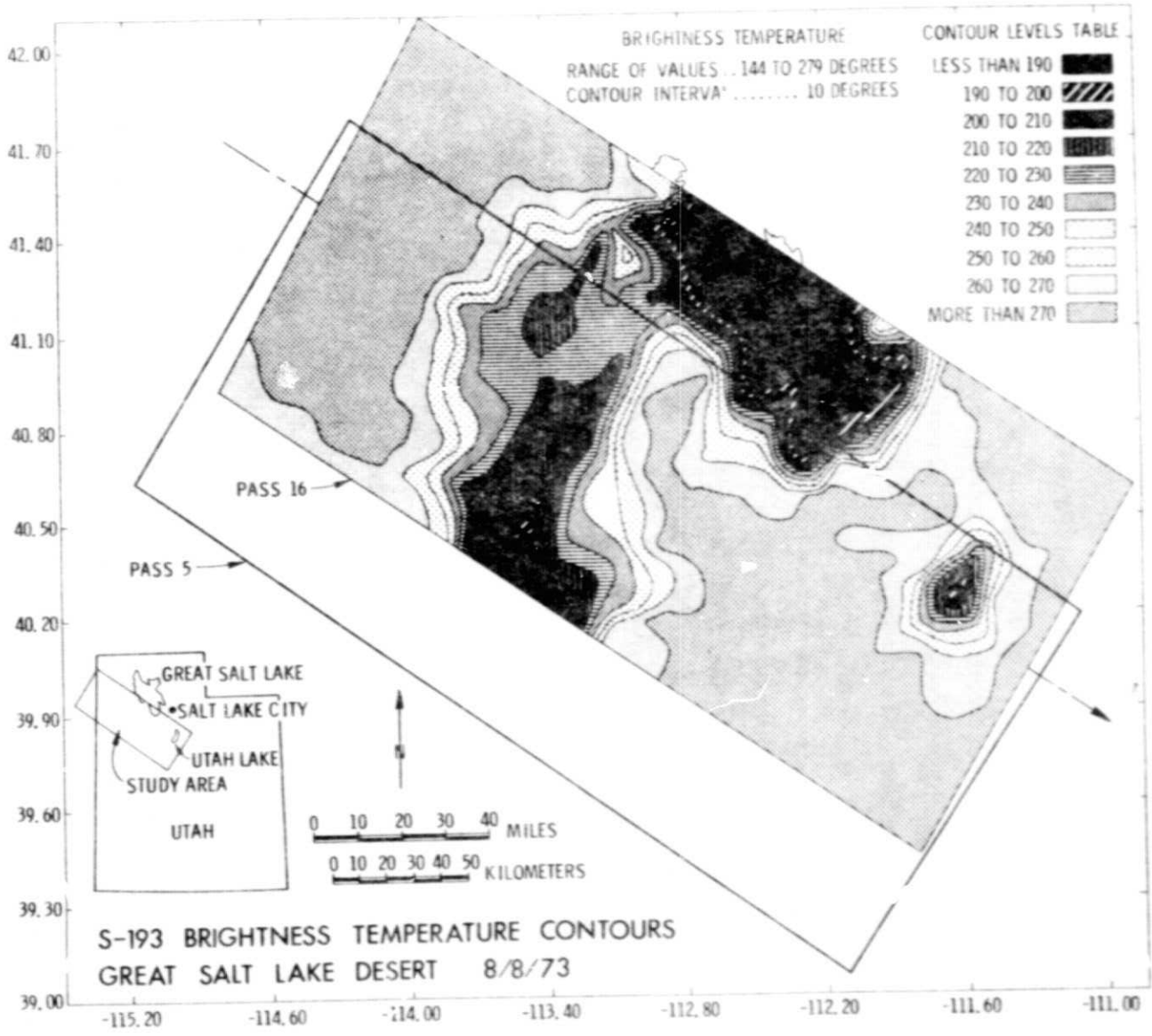

Figure 9. S-193 brightness temperature contours based on the data of Figure 8.

3.2 S-194 Observations

Simultaneous with the S-193 measurements discussed in the previous section, passive L-band (1.4 GHz) data were acquired during the same passes over Utah. The radiometer was nadir-looking having a circular footprint approximately 117 km in diameter. Ground distance covered between consecutive measurement points shown in Figure 10 is approximately 7km, producing about 94 per cent overlap. The measured data are plotted in Figure 11 as a function of distance from the center of a reference footprint. This plot represents a convolution of the ground brightness temperature (T_{BS}) spatial variation with the antenna power pattern as the latter is swept across the test site along the subsatellite track. Before crossing the desert boundary on the western side, the S-194 radiometer recorded a constant brightness temperature of 260°K for footprints 1 through 9. Between footprints 9 and 26, whose centers are separated by approximately 115 km, the brightness temperature dropped to a low of 202°K, after which it remained unchanged over the next 20 km and then it increased to a value of 252°K over the eastern section of the test site. With a 94 per cent overlap between successive footprints, the fast rate of change of the brightness temperature as the antenna beam swept across each of the two boundaries of the desert, signifies a much faster rate of change of the ground brightness temperature (T_{BS}) spatial distribution in the direction of the satellite track. The combination of S-193 and S-194 observations suggests that the lowest T_{BS} value of the desert center at 1.4 GHz must be much lower than 202°K.

Following the same basic procedure as described above, data recorded on Pass 16 (August 8, 1973) are shown in Figures 12 and 13. Figure 13 shows a plot similar in shape to the plot shown in Figure 11 although having a slightly wider range of T_B; west of the desert $T_B \approx 270°K$, east of the desert $T_B \approx 260°K$ and over the desert the lowest T_B recorded was 195°K. The difference between the brightness temperatures corresponding to footprints on the western and eastern sections of the test site (10°K) is comparable with the difference observed for Pass 5 (8°K), yet the absolute value is higher by about 10°K. Since the reported air temperature for Pass 16 is only 2°K higher than that of Pass 5, the 10°K increase in absolute value must be, for the most part, attributable to differences in the topography due to the ground separation of the two passes. The low of 195°K is attributed to partial contributions by the Great Salt Lake.

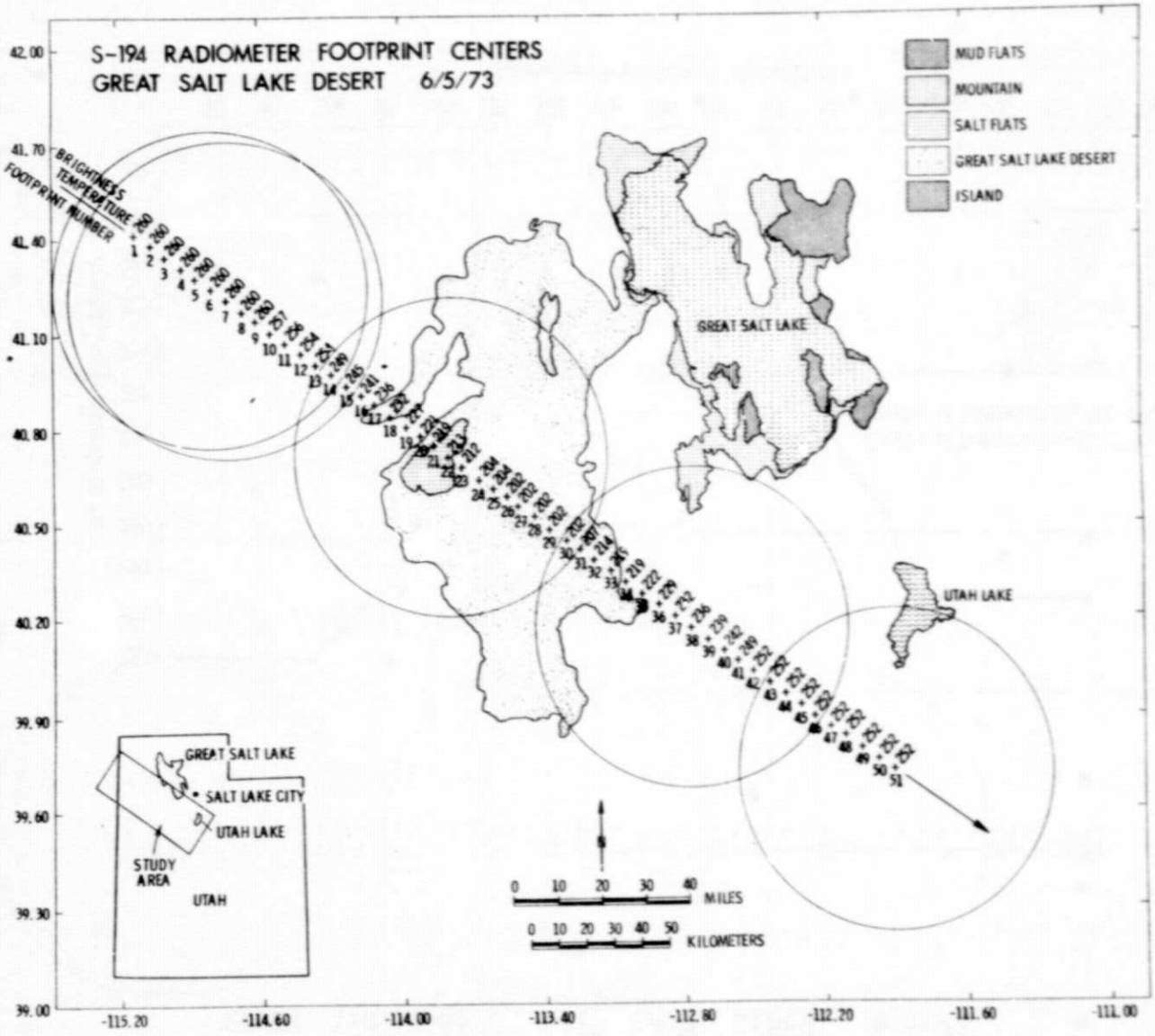

Figure 10. S-194 radiometer footprint centers, Pass 5, 6/5/73. Only footprints 6, 7, 22, 38 and 51 are shown.

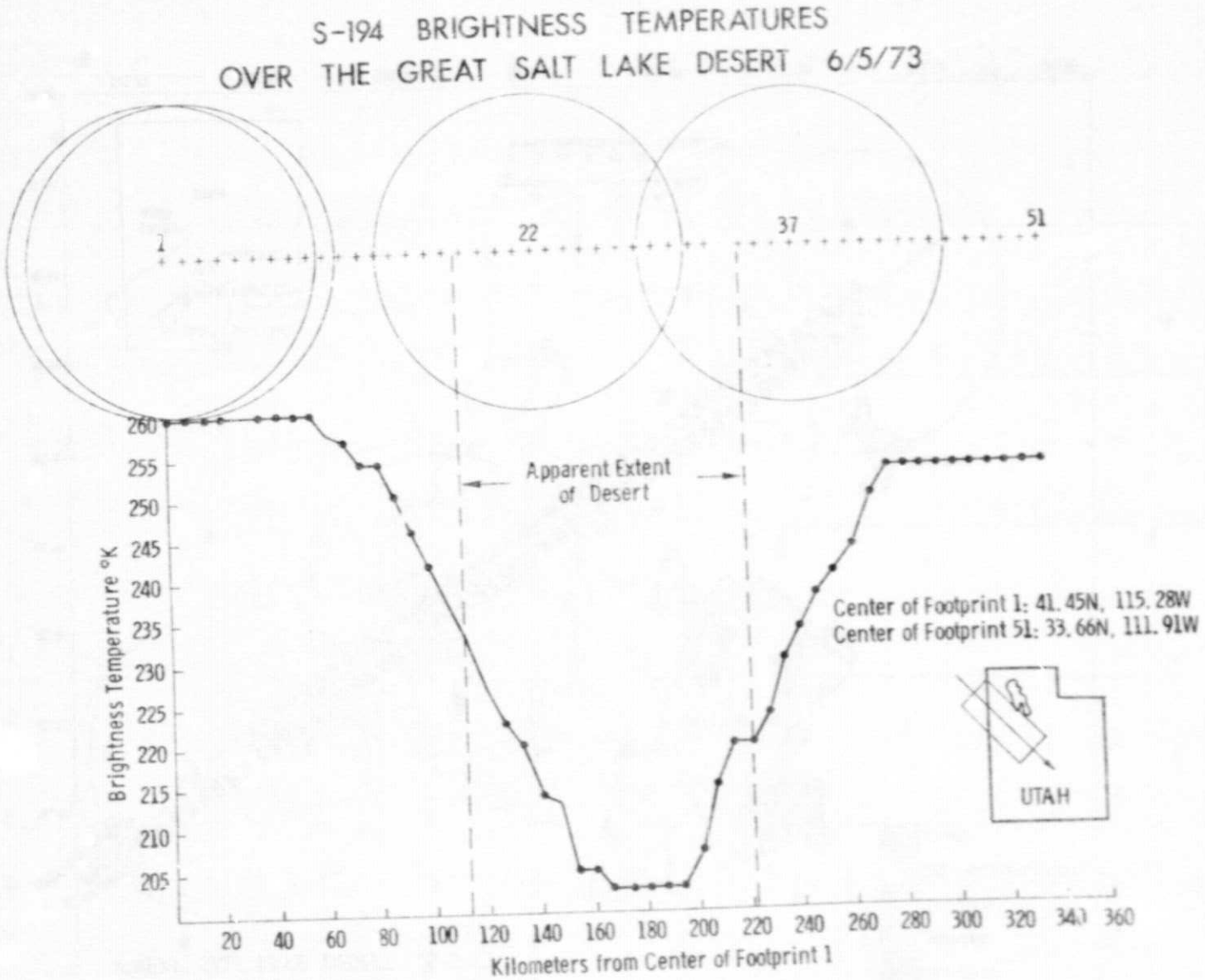

Figure 11. S-194 brightness temperature as a function of distance from the center of footprint 1 on Figure 8.

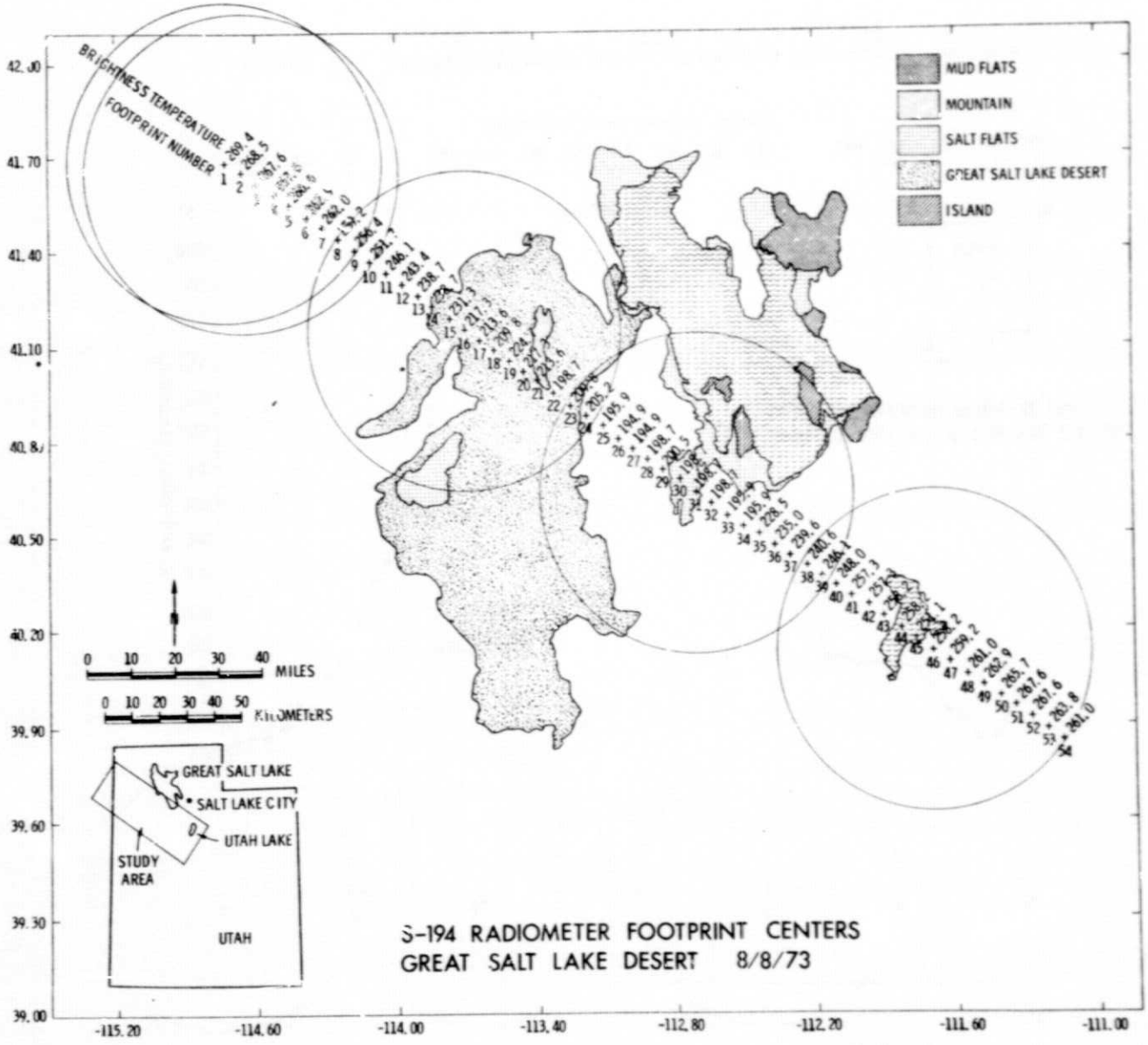

Figure 12. S-194 radiometer footprint centers, Pass 16, 8/8/73. Only footprints 1, 18, 37 and 54 are shown.

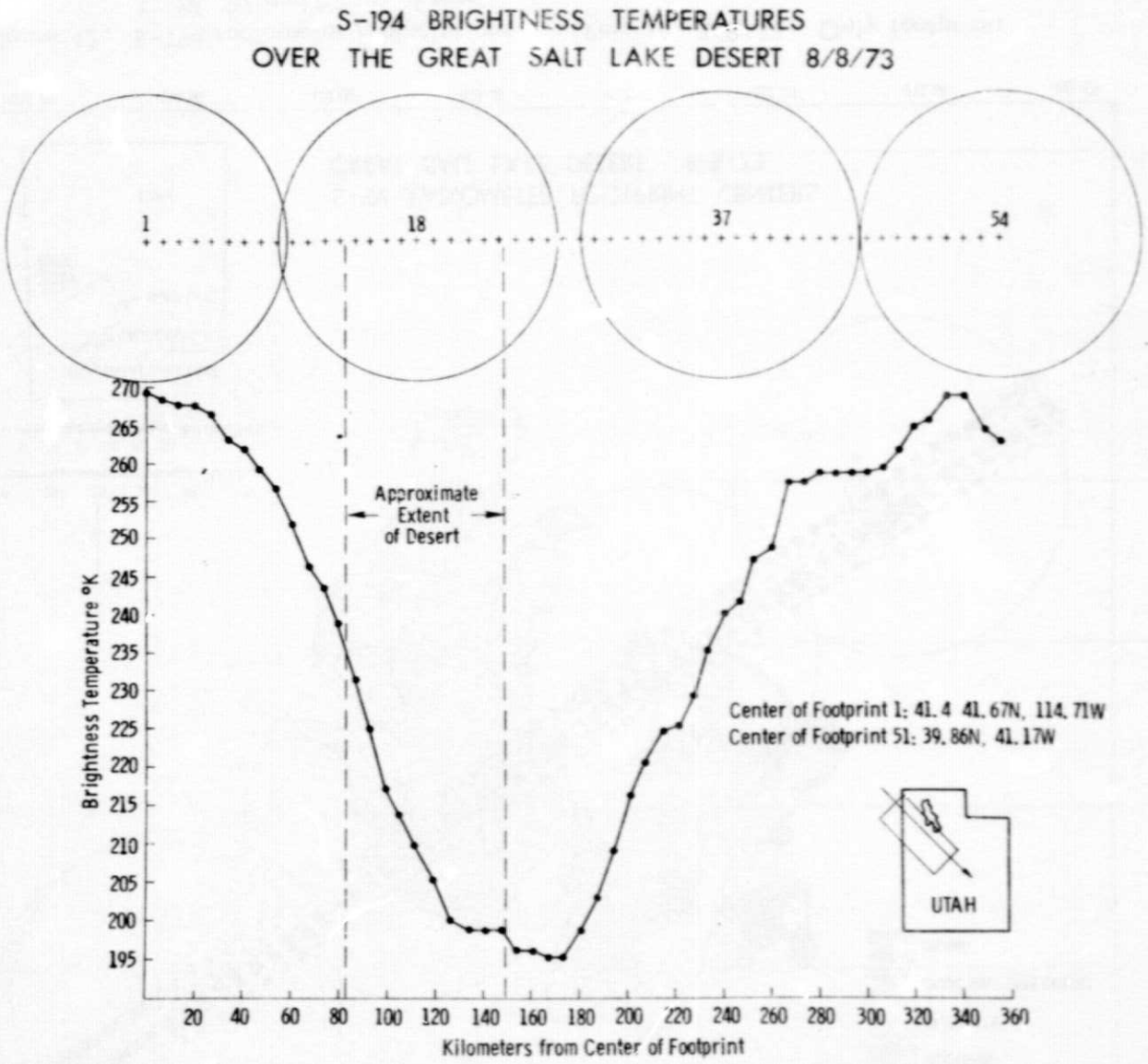

Figure 13. S-194 brightness temperature as a function of distance from the center of footprint 1 on Figure 12.

In support of Pass 16, aircraft data was acquired by NASA using the L-band portion of the Multi Frequency Microwave Radiometer (MFMR) on August 10, 1973, two days after the test site was traversed by Skylab. The course flown was a straight line from 41.275°N, 113.899°W to 40.843°N, 112.992°W, which crosses the desert along a line close to the subsatellite track of Pass 16 [NASA, 1974].

Figure 14 is a Skylab photographic image of the northern part of the Great Salt Lake Desert on which the course flown by MFMR is indicated. Also shown is a plot of the brightness temperature recorded by the MFMR instrument which indicates T_B values ranging between 285°K and 303°K over the mountains on the two ends of the pass and over the New Foundland mountains approximately half-way in between. In comparison, the brightness temperature of the desert portions of the pass are generally lower by 150°K or more. The lowest recorded T_B value was 93°K.

3.3 Nimbus 5 ESMR Observations

The Nimbus 5 satellite launched on December 11, 1972 carries an Electrically Scanning Microwave Radiometer (ESMR).

The ESMR consists of the following major components: [Wilheit, 1972]

a) A phased array microwave antenna consisting of 103 waveguide elements each having its associated electrical phase shifter. The aperture area is 83.3 cm x 85.5 cm. The polarization is linear, parallel to the spacecraft velocity vector.

b) A beam steering computer which determines the coil current for each of the phase shifters for each beam position.

c) A microwave receiver with a center frequency of 19.35 GHz and an IF bandpass of from 5 to 125 MHz; thus it is sensitive to radiation from 19.225 to 19.475 GHz, except for a 10 MHz gap in the center of the band.

The unit is arranged to scan perpendicular to the spacecraft velocity vector from 50° to the left to 50° to the right of nadir (in 78 steps) every four seconds. The beam width is 1.4° x 1.4° near nadir and degrades to 2.2° crosstrack x 1.4° downtrack at the 50° extremes. For a nominal orbit of 1100 km altitude, the resolution is 25 km x 25 km near nadir degrading to 160 km crosstrack x 45 km downtrack at the ends of the scan. The satellite orbit is polar with noon and midnight equator crossings.

MFMR BRIGHTNESS TEMPERATURE VARIATION
ACROSS THE GREAT SALT LAKE DESERT, UTAH 8/10/73

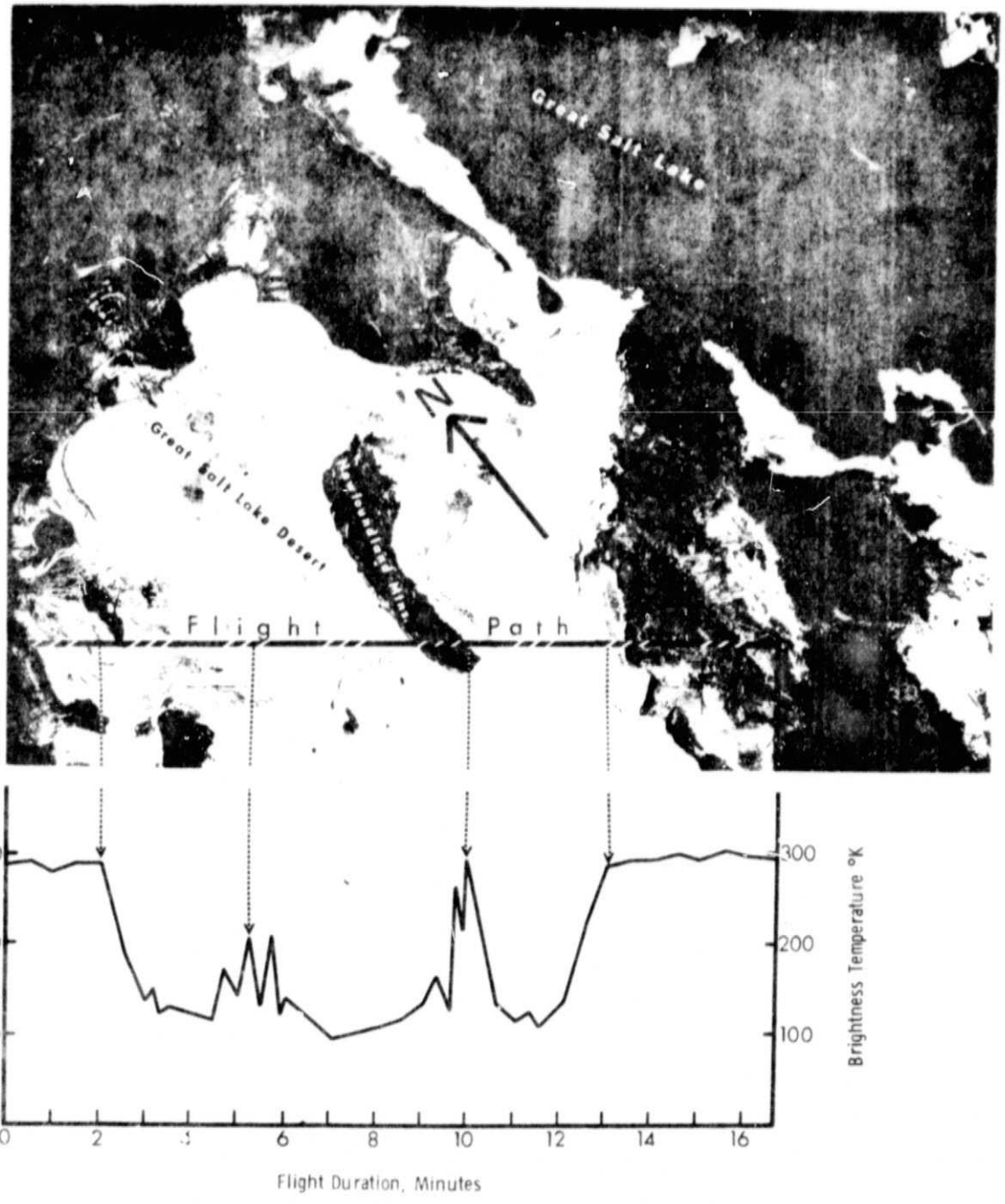

Figure 14. Skylab photographic image of the Northern portion of the Great Salt Lake Desert on which MFMR coverage on August 10, 1973 is indicated.

There is an empirical correction applied to the data for the off nadir beam positions, this correction is designed to eliminate the angular variation of brightness temperature over the ocean. To minimize the effect of this correction and the degradation of resolution, the analysis in this paper was primarily restricted to data from nadir angles of 30° or less.

A contour map of the ESMR brightness temperatures for the Great Salt Lake area is shown in Figure 15 with the outlines of the lake and desert indicated for reference . The brightness temperatures over the lake are not as low as those observed over the ocean (less than 140°K), because the width of the lake is comparable to the resolution of the instrument. Thus it is unlikely that the minimum over the desert is as low as it could be. The minimum T_B observation over the desert is about 70°K less than the surrounding areas, which were up to 280°K. On the following night, the minimum over the Great Salt Lake Desert was about the same while the observed brightness temperature over the surrounding desert dropped to below 260°K. Similar maps were produced for the area on a several per month basis from June, 1973 to December, 1974. The minimum brightness temperature observed over the desert is plotted as a function of time for that period (Figure 16). For comparison the brightness temperature of a spot (40°45'N x 114°45'W) 60 km west of Wendover is also plotted to indicate the type of seasonal variation that might be expected for the usual terrain outside the desert area. In general the brightness temperature for this location varies rather smoothly from a maximum of 280°K in July and August down to a minimum of 240°K for January and February and appears to repeat from one year to the next. The minimum brightness temperature over the Great Salt Lake Desert followed a similar sort of seasonal variation with its maximum occurring in July and August. However, the minima were in November in response to the fall rains during both years. There is a significant difference in the level of the brightness temperature for the summers of 1973 and 1974. The minimum temperatures observed over the Great Salt Lake Desert in the summer of 1974 were 20°-30°K higher than those observed during the summer of 1973. The rainfall during the summer of 1974 was only 50 per cent of normal while in 1973 it was slightly above normal. The average monthly rainfall for eight stations surrounding the basin is shown as bar graphs on the bottom of this figure and clearly indicates this difference in rainfall for the two summers. The response to the heavier fall rains of November, 1973 and October, 1974 is indicated and in particular the lowest brightness temperature was observed on 18 November 1973 when more than 1 cm of rain was recorded at the

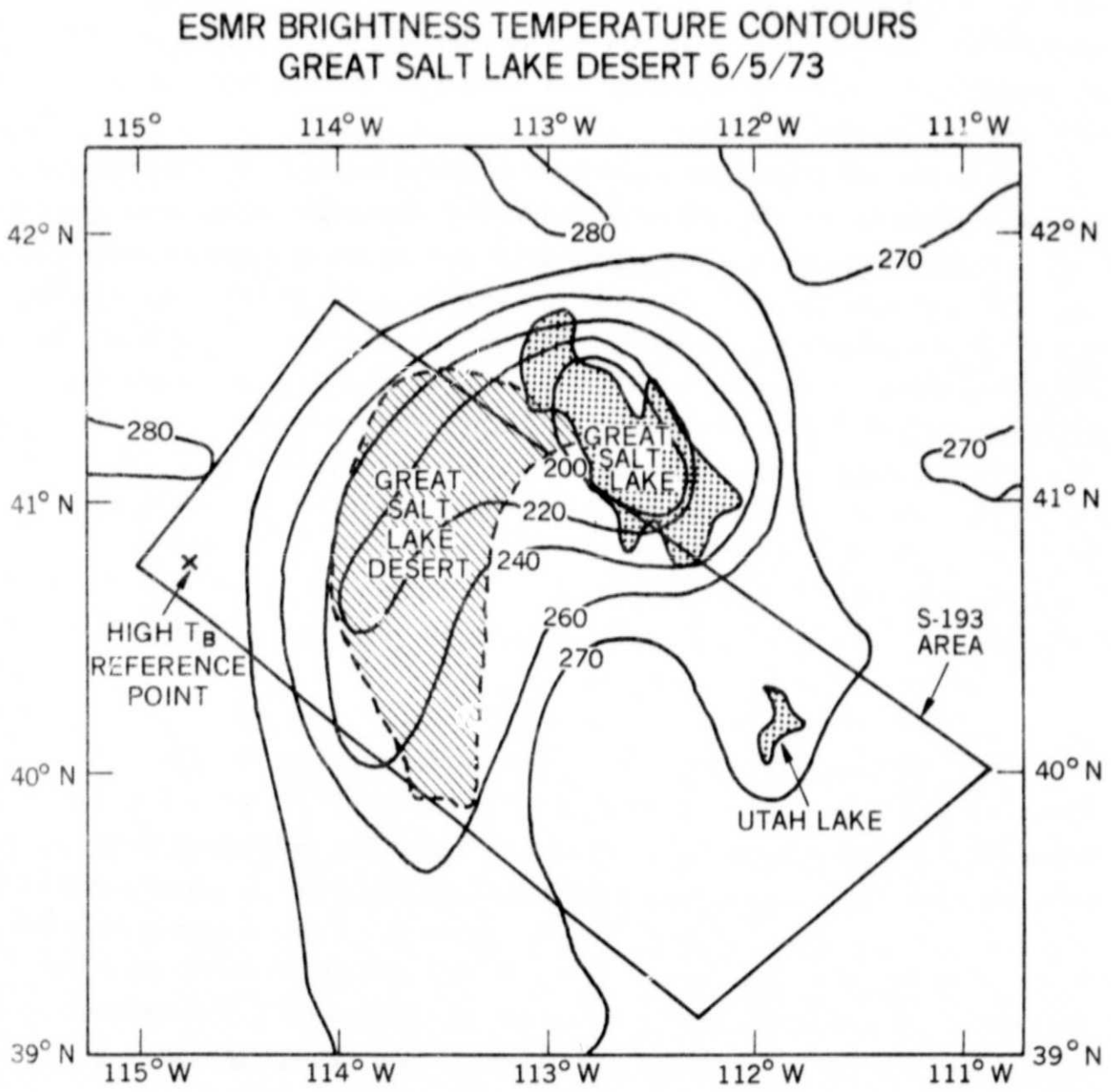

Figure 15. ESMR brightness temperature contours, 6/5/73.

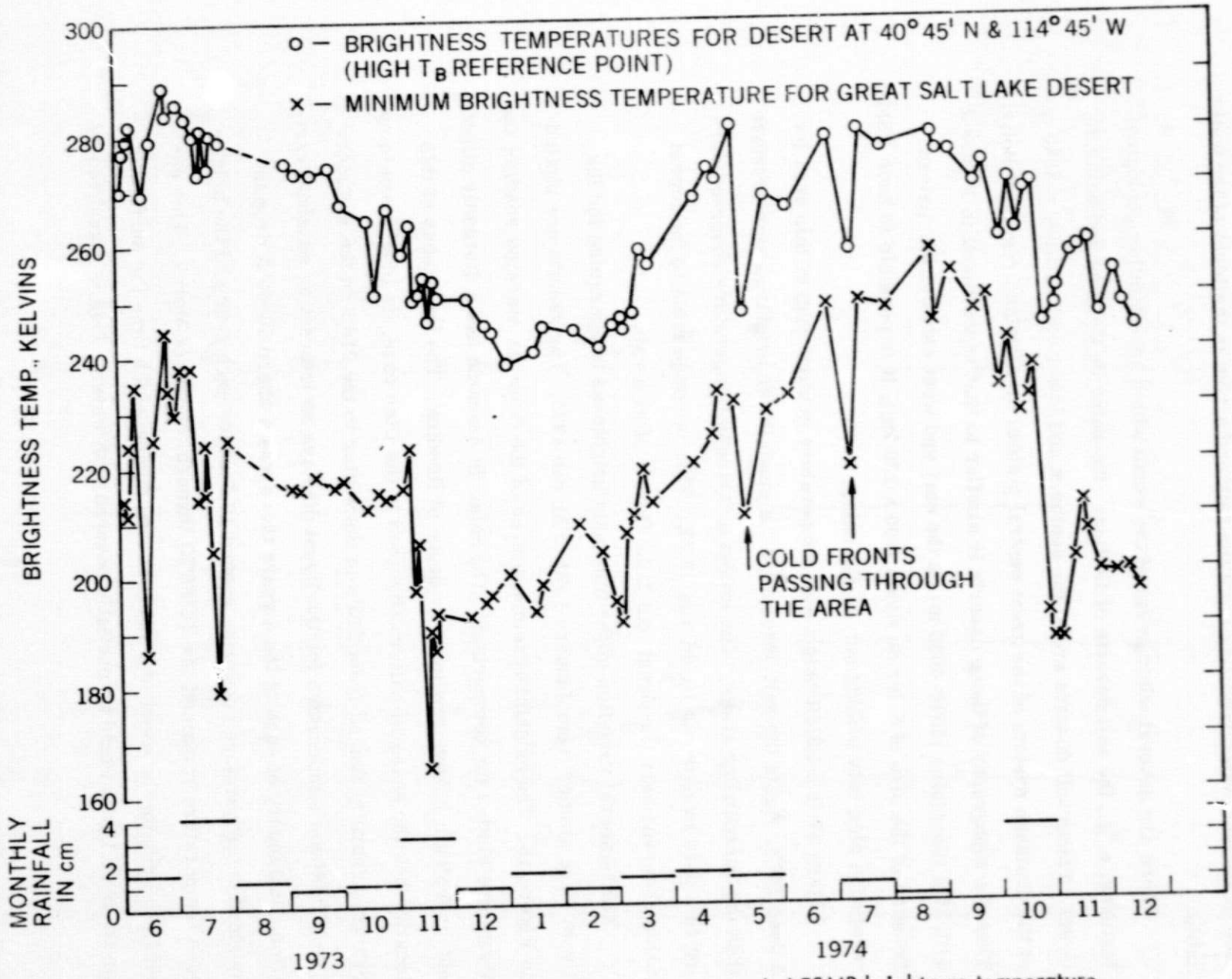

Figure 16. Temporal variations of the minimum recorded ESMR brightness temperature over the Great Salt Lake Desert (x) compared with the ESMR brightness temperature (o) of the reference point outside the desert (indicated in Figure 11).

eight stations. It appears that the radiometer may be responding to a combination of surface water resulting from the rain and a rise in the level of the water table.

There are several other areas of the world which have similar geological features, e. g., the salt deserts of Bolivia: the Salar de Coipasa and Salar de Uyuni. These salt deserts are at the southern and lower end (altitude = 3660 m) of the drainage system of the great central plateau or Altiplano region of Bolivia. Thus the topography of these deserts is similar to that represented in Figure 2 with high mountains (5000-6000 m) on the east and west sides of the plateau. Because of the size of Salar de Uyuni (100 x 120 km), it is possible to have ESMR resolution elements looking only at the Salar.

Figure 17 is a ESMR brightness temperature contour map of this area for 6 June 1973. Again the salt deserts have a much lower brightness temperature than the surrounding areas. The lowest brightness temperature observed during this pass over the de Uyuni was 165°K. This is comparable to the lowest value observed over the Great Salt Lake Desert after a rain.

The temporal variation of the minimum brightness temperature for the Uyuni were studied from January 1973 to March 1975. The results are plotted in Figure 18. The brightness temperatures of the Salar de Atacama south of the Uyuni are plotted for comparison. The Salar de Atacama has a distinctly different hydrologic behavior with no evidence of flooding. The brightness of this location has the seasonal pattern observed in the Utah case, its brightness temperature generally ranged from 240's in the winter to the 270's in the summer. The brightness temperature for the Uyuni displays an interesting seasonal variation. In January of each of the 3 years there was a sharp 50-60°K drop in brightness temperature occurring around 10 January each year and the brightness temperature remained low (<160°K) through the end of March. This appears to indicate the onset of a rainy season during which time the surface of the Salar de Uyuni would be partially covered with water. This is supported by

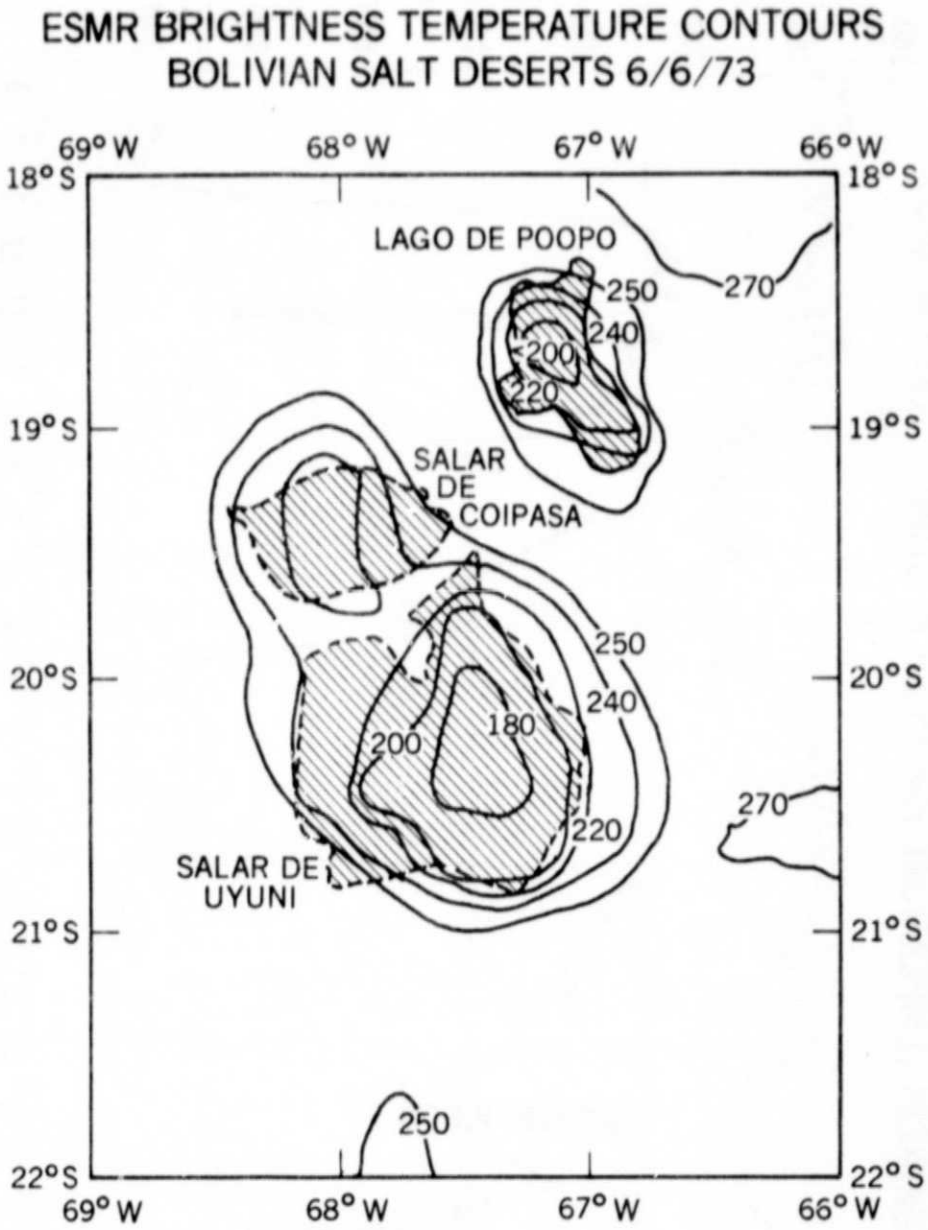

Figure 17. ESMR brightness temperature contours of the Bolivian salt deserts, 6/6/73.

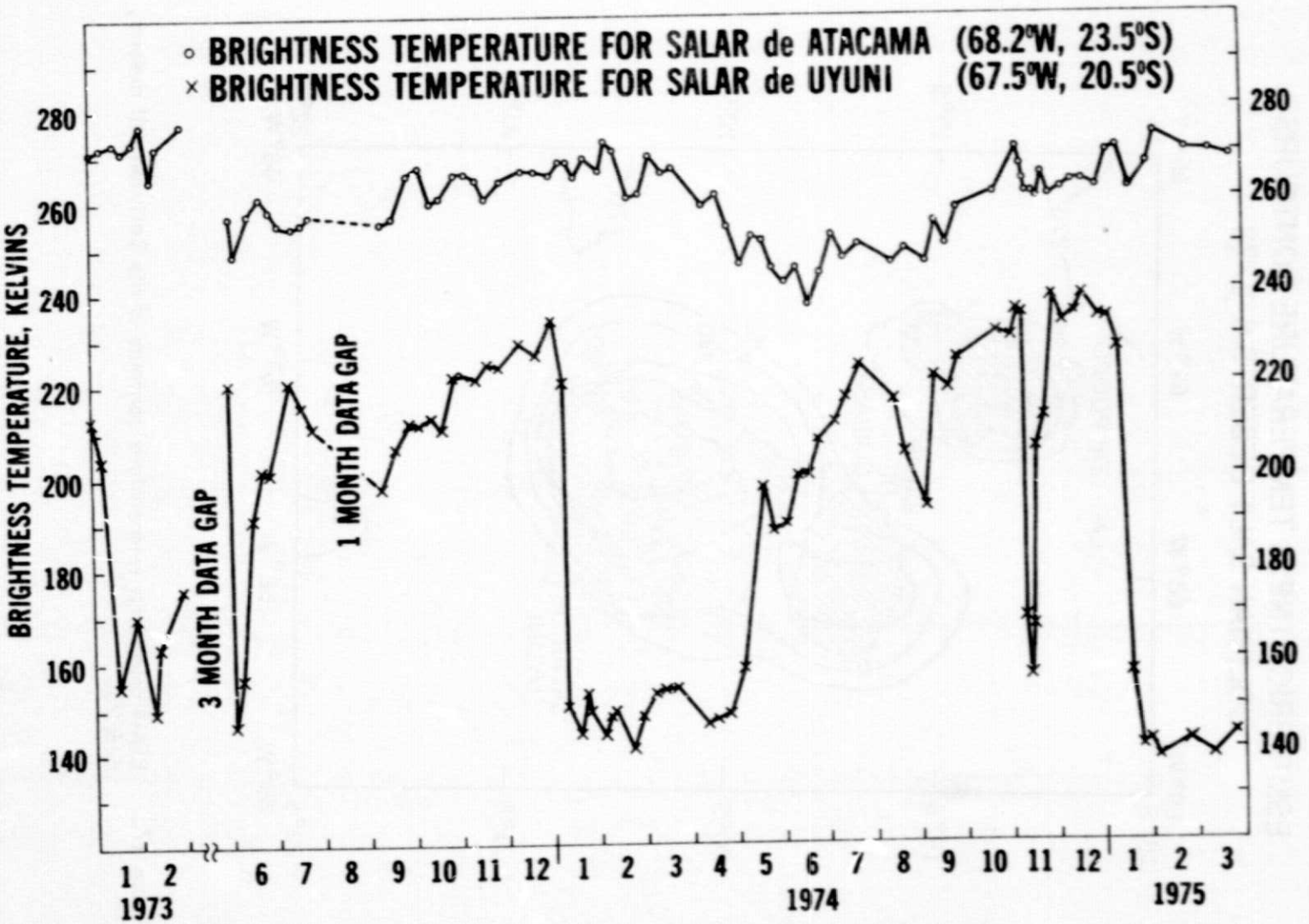

Figure 18. Temporal variations of the minimum recorded ESMR brightness temperature over the Salar de Uyuni and the Salar de Atacama.

the precipitation data for Oruro (18°S, 67°W), the closest station listed in the Monthly Climatic Data for the World, which indicate that the summer is the rainy period for this area.

The low brightness temperatures observed in early June 1973 and early November 1974 appear to be transitory events, i.e. following a heavy rain. The brightness temperatures in these instances remained low for only 4 or 5 days before rising sharply. Unfortunately, detailed rainfall data are unavailable for verification.

The brightness temperatures observed for December 1973 (<230) were about 10°K less than those for December 1974. This perhaps indicates that 1974 had been a drier year than 1973, but there is no rainfall data to verify this.

There have been 3 Landsat I passes over the area: August 1972; October 1972; and March 1973. The first two were before the Nimbus 5 launch and were for the dry period; the third one was during the period when the ESMR was malfunctioning. This last pass was the most interesting because of the indications of water along the northern and eastern shores of the Salar. The ESMR data for March of 1974 and 1975 indicate that a larger portion of the Salar is covered with water than indicated in the Landsat imagery of March 1973.

The brightness temperature of the Salar during the dry season of the year is in the 220-240°K range, and is at least 20°K lower than the surrounding terrain. The gradual raise of brightness temperature from September to December of each year is perhaps the result of a gradual lowering of the water table. This behavior is similar to that observed over the Utah desert.

4.0 CONCLUDING REMARKS

Comparison of the microwave data acquired by Skylab, Nimbus and MFMR with the available information on the hydrology of the Great Salt Lake Desert suggests the following conclusions:

a) Subsurface water exhibits a strong influence on the measured scattering coefficient and brightness temperature, particularly over the central part of the desert where the water table is the closest to the surface. Although this influence is clearly discernible at 13.9 GHz and 19.35 GHz, it is most pronounced at 1.4 GHz; over the desert the minimum recorded brightness temperature by the L-band channel of the airborne MFMR radiometer was 93°K in comparison to 285°K-303°K over the mountains.

b) According to the calculated emissivity of saline soil (with 150 °/oo) at 1.4 GHz (Table 1), it is not surprising that the 93°K brightness temperature recorded by MFMR is lower than the brightness temperature of water at the same frequency and ground temperature. For T_g = 296°K, $T_{BS} = \epsilon_{ss} T_g = 80.65°K$. The presence of the surface layer above the brine increases T_{BS} to a higher temperature.

c) The configurations of the brightness temperature contours of the S-193 radiometer and the Nimbus 5 Electrically Scanning Microwave Radiometer are in agreement with the reported variation of the depth of the water table below the surface between the central part of the desert and the desert margins.

REFERENCES

Bagley, J. M., R. W. Jeppson, and C. H. Milligan, 1964, Water yields in Utah, Utah Agr. Expt. Sta. Spec. Rept. 18, Utah State Univ., Logan, Utah, p. 55.

Busby, M. W., 1966, Annual runoff in the conterminous United States, U. S. Geological Survey Hydrol. Inv. Atlas HA-212, 1 sheet. U. S. Geol. Survey, Room 8102 Federal Bldg., 125 South State Street, Salt Lake City, Utah, 94138.

Eagleman, J. and F. T. Ulaby, 1974, Remote sensing of soil moisture by Skylab radiometer and scatterometer sensors, Advances in the Astronomical Sciences, vol. 31, the American Astronomical Society, Tarzana, California, August.

Eardley, A. J., 1962, Gypsum dunes and evaporite history of the Great Salt Lake Desert, Utah Geol. and Mineralog. Survey Spec. Studies 2, p. 22. Utah Geological and Mineralogical Survey, 103 Utah Geol. Survey Bldg., Univ. of Utah, Salt Lake City, Utah.

Hookstra, P. and A. Delaney, "Dielectric Properties of Soils at UHF and Microwave Frequencies," Journal of Geophysical Research, vol. 79, no. 11, pp. 1699-1708, April, 1974.

King, D. D., 1970, Passive derection, Chapter 39 of Radar Handbook, Edited by M. I. Skolnik, Mc-Graw Hill, New York, p. 39-9.

Moore, R. K., 1975, Microwave remote sensors, Chapter 9, vol. 1 of the Manual of Remote Sensing, Edited by F. Janza, American Society of Photogrammetry, Falls Church, Virginia.

NASA, 1974, Skylab program: Earth resources experiment package, sensor performance report, vol. 6 (S194), MSC-05528, Lyndon B. Johnson Space Center, Houston, Texas, September, pp. 1-1 to 9-45.

Newton, R. W., S. L. Lee, J. W. Rouse, Jr. and J. F. Paris, 1974, On the feasibility of remote monitoring of soil moisture with microwave sensors, Proc. Ninth Intl. Symp. on Remote Sensing of Environment, Environmental Research Institute of Michigan, Ann Arbor, Michigan, April, pp. 725-738.

Nolan, T. B., 1928, Potash brines in the Great Salt Lake Desert, Utah in: Loughlin, G. F. and G. R. Mansfield Contributions to Economic Geology, Part I--Metals and Nonmetals Except Fuels, U. S. Geological Survey Bulletin 795, p. 41. U. S. Geol. Survey, Room 8102 Federal Bldg., 125 South State Street, Salt Lake City, Utah, 84138.

Schmugge, T., P. Gloersen, T. Wilheit, and F. Geiger, 1974, Remote sensing of soil moisture with microwave radiometers, Journal of Geophysical Research, vol. 79, no. 2, pp. 317-323.

Sobti, A., 1973, A simulation study of the S-193 RADSCAT in orbit, RSL Technical Report 190-2, University of Kansas Center for Research, Inc., Remote Sensing Laboratory, Lawrence, Kansas, May, pp. 1-140.

Stephens, J. C., 1974, Hydrologic reconnaissance of the Northern Great Salt Lake Desert and summary hydrologic reconnaissance of Northwestern Utah, U. S. Geological Survey Tech. Publ. No. 42, Utah Dept. of Natural Resources, 442 State Capitol, Salt Lake City, Utah, pp. 3-18.

Stogryn, A., 1971, Equations for calculating the dielectric constant of saline water, IEEE Trans. on Microwave Theory and Techniques, vol. MTT-19, no. 8, August, pp. 733-736.

Ulaby, F. T., 1974a, Radar measurement of soil moisture content, IEEE Trans. on Antennas and Propagation, vol. AP-22, no. 2, pp. 257-265.

Ulaby, F. T., J. Barr, A. Sobti and R. K. Moore, 1974b, Soil moisture detection by Skylab's microwave sensors, Proc. URSI Specialist Meeting on Microwave Scattering and Emission from the Earth, Institute of Applied Physics, University of Berne, Berne, Switzerland, pp. 205-208.

Ulaby, F. T., J. Cihlar and R. K. Moore, 1975a, Active microwave measurement of soil water content, Remote Sensing of Environment, vol. 3, pp. 185-203.

Wilheit, T., 1972, The electrically scanning microwave radiometer (ESMR) experiment, in: The Nimbus 5 User's Guide, NASA Goddard Space Flight Center, Greenbelt, Maryland, November, pp. 59-105.